International Journal of Innovative Scientific & Engineering Technologies Research 14(3):145-168, July-Sept, 2026

© SEAHI PUBLICATIONS, 2026 www.seahipublications.org ISSN: 2360-896X

DOI:10.5281/zenodo.22663962

First-Principles Investigation Of The Structural Properties And Numerical Convergence Of Group 13 Nitrides

[1]Mahmud Abdulsalam, [2]Auwal Abdulkadir, [3] Nura Liman Chiromawa, [4] Suleiman Shuaibu,

[1-3]Department of Physics, Umaru Musa Yar'adua University, Katsina, Nigeria.
[3]Department of Physics, Al-qalam University, Katsina, Nigeria.
Emails: suleman2014k3@gmail.com/sulemanshuaibu@auk.edu.ng

ABSTRACT
This study investigates the structural stability and computational convergence of Group 13 nitrides, namely boron nitride (BN), aluminum nitride (AlN), gallium nitride (GaN), indium nitride (InN), and thallium nitride (TlN), using Density Functional Theory (DFT) as implemented in the Quantum ESPRESSO package. The calculations employed the Perdew–Burke–Ernzerhof generalized gradient approximation (PBE-GGA), plane-wave basis sets, ultrasoft pseudopotentials, and Monkhorst–Pack k-point sampling. Self-consistent field (SCF), plane-wave cutoff-energy, and k-point convergence tests were performed to establish reliable computational parameters, while equilibrium lattice parameters were obtained from the minimum of the total-energy curves. The SCF calculations demonstrated stable convergence for all five nitrides, with the total energies stabilizing rapidly after approximately three iterations. The final converged energies were −52.41361132 Ry for BN, −48.36054160 Ry for AlN, −197.76204781 Ry for GaN, −156.46760884 Ry for InN, and −273.11210465 Ry for TlN. The cutoff-energy tests revealed stable regions around 118–136 Ry for BN, 80–105 Ry for GaN, 35–42 Ry for InN, 97–109 Ry for TlN, and approximately 45 Ry for AlN. K-point tests similarly demonstrated the importance of adequate Brillouin-zone sampling, although further quantitative convergence testing was indicated for some materials. The calculated equilibrium lattice parameters were approximately 2.40 Å for BN, 3.95 Å for AlN, 3.09 Å for GaN, 3.60 Å for InN, and 3.615 Å for TlN. The results demonstrate that systematic convergence testing and total-energy minimization provide a reliable basis for determining the structural parameters of Group 13 nitrides and for subsequent electronic and optical-property calculations.

Keywords: Group 13 nitrides; Density Functional Theory; Quantum ESPRESSO; SCF convergence; plane-wave cutoff; k-point convergence; lattice parameter.

1.0 INTRODUCTION

The urgent need for clean and dependable electricity has increasingly driven communities to embrace renewable energy technologies such as solar panels, solar cells, and inverters. In this context, group 13 nitrides; have emerged as critical materials that enhance the efficiency and performance of solar energy systems. These compounds possess wide and tunable band gaps, high thermal stability, and excellent electron mobility, making them ideal for high-efficiency solar cells and power electronic devices like inverters (Wu, 2009; Ueda et al., 2014). For example, some of these materials are based inverters enable faster switching and reduced energy loss compared to traditional silicon devices, thereby improving the

overall efficiency of electricity conversion in solar power systems (Jain et al., 2000). These nitride families are being explored for next-generation photovoltaic devices due to their strong light absorption and potential to cover a broad solar spectrum (Wu, 2009). To this regard, integrating nitrate semiconductors into solar technologies not only supports the global transition to clean energy but also helps deliver affordable, sustainable, and high-performance electricity to both urban and remote communities (Kabir et al., 2018; IRENA, 2020; Cheng et al., 2018).

Group 13 nitrides, comprising compounds formed between Group 13 elements (boron, aluminum, gallium, indium, and thallium) and nitrogen, represent a class of materials critical to advancements in modern electronics, optoelectronics, and advanced materials research(Andreev et al., 2018). These compounds are distinguished by their robust covalent bonding, exceptional thermal stability, and a broad spectrum of electronic properties, ranging from wide bandgap insulators to direct-gap semiconductors (Andreev et al., 2018). While most Group 13 nitrides predominantly crystallize in the hexagonal wurtzite structure, such as aluminum nitride (AlN), gallium nitride (GaN), and indium nitride (InN), boron nitride (BN) exhibits a rich polymorphism with several allotropes. Thallium nitride (TlN), though less extensively studied, is theoretically predicted to possess distinct structural and electronic behaviors that set it apart from its lighter counterparts (Li, 2023). Their unique combination of properties, including wide bandgaps, high thermal conductivity, and excellent chemical stability, positions Group 13 nitrides as indispensable materials for high-power, high-frequency, and optoelectronic devices. The ability to engineer their properties through alloying and nanostructuring further expands their utility, driving innovation across various technological domains. This document provides a detailed overview of each Group 13 nitride, focusing on their crystallographic space groups, key physical and electronic properties, and diverse applications (Rinke et al., 2006).

The ongoing DFT research in these areas drives innovation, addresses critical technological challenges and contributes to a more sustainable and technologically advanced future by enabling new generations of communication, energy and computing solutions (Cheng et al., 2018; Perdew et al., 1996; Singh et al., 2021).

Experimental investigations of these nitrides are often limited by synthesis complexities, material defects, strain effects, and measurement inaccuracies, which complicate the interpretation of fundamental properties such as bandgap energy, carrier mobility, and optical absorption spectra (Wu et al., 2002; Cassabois, Valvin, & Gil, 2016). For instance, InN suffers from significant surface electron accumulation, leading to inaccurate bandgap estimation, while BN exists in several polymorphs (e.g., h-BN, c-BN, w-BN), each with markedly different properties that are difficult to isolate experimentally (Lu et al., 2005; Wirtz et al., 2006).

Therefore, there is a pressing need for a systematic and accurate DFT-based study that investigates and compares the structural, electronic, and optical properties of the main crystalline phases of BN. Such a study would not only contribute to the fundamental understanding of this technologically important material but also guide the design and integration of BN in electronic and photonic devices. The aim of this research is to investigate the structural properties of Aluminum Nitride (AlN), Gallium Nitride (GaN), Indium Nitride (InN), and Boron Nitride (BN) as predicted by Density Functional Theory (DFT)

2.0 CONCEPTUAL FRAMEWORK

Many-Body Problem

The many-body problem refers to the problem of solving the Schrodinger equation for a system of atoms and electrons. Quantum mechanics is a mathematical tool for predicting the behaviors of microscopic particles. In fact, one of the advantages of quantum mechanical calculations is its ability to predict the total energy of a system of electrons and nuclei. The rules of calculating the energies of the complicated systems are the extension of those for simple one-atom systems. Having found the total energy of system, the instances are the equilibrium lattice constant that minimizes the total energy, or the fact that the surfaces and defects of solids adjust themselves in a way that minimize the related total energies. If total energies are calculated precisely, most of the physical properties can be estimated. Hence, electronic and

geometric structure of solids can be predicted by total energy calculations and the relevant minimizations with respect to the electronic and nuclear coordinates. [Noei, et al., 2013]

However, the Schrodinger equation, which is the central equation of energy calculation, is too complicated to be solved analytically for all but the simplest (and hence most trivial) systems; it is exactly solvable just for harmonic oscillator, two particle system such as Hydrogen atom (analytically), and a very-few-particle systems (numerically). The only way of using the power of quantum mechanics is to solve the equations numerically by modeling the processes of interest computationally. [Liu, et al 2014]

The properties of a many-body quantum system are formulated in many-body Schrodinger equation. The simplest form of time-independent Schrodinger equation is:

$$\hat{H}\Psi_I(\vec{x}_1,\vec{x}_2,\dots.,\vec{x}_N,\vec{R}_1,\vec{R}_2,\dots,\vec{R}_M) = E\Psi(\vec{x}_1,\vec{x}_2,\dots.,\vec{x}_N,\vec{R}_1,\vec{R}_2,\dots,\vec{R}_M) \quad (1)$$

The Hamiltonian of a system of electrons and nuclei is given by:

$$\hat{H} = \frac{-\hbar^2}{2m_e}\sum_i \nabla_i^2 + \sum_{i,I}\frac{-Z_i e^2}{|\vec{r}_i-\vec{R}_I|} + \frac{1}{2}\sum_{i\neq j}\frac{e^2}{|\vec{r}_i-\vec{r}_j|} - \sum_I \frac{\hbar^2}{2M_I}\nabla_i^2 + \frac{1}{2}\sum_{I\neq J}\frac{Z_I Z_J e^2}{|\vec{R}_I-\vec{R}_J|} \quad (2)$$

Where $\hbar$ is the reduced Plant constant, e is the electron charge, Z is the nuclei charge and electron and nuclei properties are shown by lower case and upper case respectively. The first term is the electronic kinetic energy, the second term is electron-nuclei Coulomb attraction, the third term is the electron-electron repulsion, the fourth term is the nuclear kinetic energy and the last term is nuclei-nuclei repulsion. In the presence of external electric or magnetic fields, Hamiltonian may contain even more terms. [Sun, et al., 2014]

The above Hamiltonian can be written in the following form:

$$\hat{H}=\hat{T}_e + \hat{V}_{N-E} + V_{e-e} + \hat{T}_N + \hat{V}_{N-N} \quad (3)$$

The above equation is Schrodinger equation in the second order differential equation. Solving quantum mechanics quantitatively requires several approximations, of which the most widely used is independent-electron approximation such as LDA and GGA. Within this approximation each electron move independently of the others, except that the electrons obey the exclusion principle and each move is some average effective potential which may be determined by the other electrons Solozhenko I. [2001].

2.2 THEOROTICAL BACKGROUND

Hohenberg-Kohn Theorems

The Hohenberg and kohn theorems deal with any system made up of electrons that are moving under the influence of an external potential $Ve(r)$, where r is the electron nucleus-distance. These theorems are the basis of DFT and they are given as:

Theorem I

The external potential $Ve(r)$ and hence the total energy is a unique functional of the electron density $n(r)$. The energy functional $[(r)]$ mentioned in Theorem I above can be written in terms of the external potential $Vext(r)$ as

$$E[n(r)] = \int n(r)V_{ext}(r)dr + F[n(r)] \quad (4)$$

where $[(\boldsymbol{r})]$ is an unknown, but universal functional of the electron density $(\boldsymbol{r})$only.

Theorem II

The ground state energy can be obtained variationally: the density that minimizes the total energy is the exact ground state density.

The functional $[(r)]$has its minimum when the electron density is at the equilibrium electron density $n_0(r_0)$. The minimum of the energy E_0 is exactly equal the true ground-state energy,

$$E_0 - E[n(r)] = E[n_0(r_0)] \quad (5)$$

The Hohenberg-Kohn theorems are powerful but they have some limitations in that they do not provide a way of computing the ground-state density of a system in practice. Kohn and Sham came up with a simpler method of performing DFT calculations as a result Kohn W.and Hohenberg P. [1963].

2.3 Kohn-Sham Formulation

Kohn and Sham made the density functional theory as a practical tool to find the exact properties of many-body system. In 1965, Kohn and Sham proposed the idea of replacing the kinetic energy of the interacting electrons with that of an equivalent non-interacting system to facilitate the process of calculation. They assumed that the equivalent non-interacting system, called as "non-interacting reference system" and also "non-interacting-V-representability, has the same ground state density as the original interacting one. They proposed to use orbitals in such a way that the kinetic energy can be simply calculated with good accuracy, leaving a small term that is approximated separately. Kohn and Sham [1964]

3.0 METHODOLOGY

This section presents the theoretical foundation, computational methods, and tools used in the study of the structural, electronic, and optical properties of group III–V nitride semiconductors: Aluminum Nitride (AlN), Gallium Nitride (GaN), Boron Nitride (BN), Thallium Nitride (TIN) and Indium Nitride (InN). The research is based on Density Functional Theory (DFT), implemented using Quantum ESPRESSO, a widely adopted open-source computational package. All materials will be studied in their most thermodynamically stable forms: wurtzite structure for AlN, GaN, and InN, and hexagonal and cubic phases for BN.

3.1 Density Functional Theory DFT

Density functional theory (DFT) is a computational quantum mechanical modeling method used in physics, chemistry and materials science to investigate the electronic structure or nuclear structure of many body systems in particular atoms, molecules, and the condensed phases Kohn W.and Hohenberg P. [1963]. The concept of density functional theory (DFT) was conceived in 1 960s by Hohenberg, Kohn and Sham [1964] but the concept only became popular in the 1980s. Thereafter, DFT has become a standard tool for predicting the electronic properties of materials. In DFT, the electronic density distribution $n(r)$ is considered to be the basic property of a many-electron wave function Ψ Shishkin, M., & Kresse, G. [2007].

3.2 Computational Method

In this particular work, the calculations are performed on the primitive cell of aluminum nitride, boron nitride, gallium nitride and indium nitride using first principle calculation based on density functional theory (DFT), as implemented in the Quantum Espresso simulation package. Quantum ESPRESSO is an integrated software suite for atomistic simulation based on electronic structure, using density- functional theory (DFT), a plane wave (PW) basis set and pseudo-potentials (PP) (norm-conserving, ultra-soft and projector-augmented wave) [Paola et al., 2009]. The acronym ESPRESSO stands for opEn-Source Package for Research in Electronic Structure, Simulation and Optimization.

The Perdew-Burke-Ernzerhof generalized gradient approximation (PBE-GGA) scheme has been employed in approximating the exchange-correlation potential [Perdew et al., 1996]. The plane wave basis sets with the maximum kinetic energy has been used to expand the wave functions. The electron-ion

core interaction is treated by ultra-soft pseudopotentials for AlN, BN, GaN TIN and InN valence orbitals as all in the pseudo potential files. For integrals, smearing has been adopted and to be specific Maxfessel-Paxton smearing method with small Gaussian spreading has been used. The Brillouin zone integration is performed using Monkhorst-Pack scheme with k-points grids Monkhorst H. and Pack, J. [1976].

4.0 RESULTS AND DISCUSSION

This section presents and discusses the computational results obtained from the first-principles calculations carried out on the Group 13 nitrides, namely boron nitride (BN), aluminium nitride (AlN), gallium nitride (GaN), indium nitride (InN), and thallium nitride (TlN). The calculations were performed within the framework of Density Functional Theory (DFT) using the Quantum ESPRESSO package. The results are presented systematically to provide a comprehensive understanding of the physical characteristics of each material. The structural analysis includes the optimized lattice parameters, equilibrium crystal structures, unit-cell volumes, and total energies obtained after geometry optimization. These parameters provide insight into the structural stability of the materials and serve as the basis for the subsequent electronic and optical calculations.

4.1 Self-Consistent Field (SCF) Convergence Analysis of Group 13 Nitrides (BN, AlN, GaN, InN and TlN)

The first objective of this study was to obtain a stable and converged electronic ground state for the investigated Group 13 nitrides, namely boron nitride (BN), aluminium nitride (AlN), gallium nitride (GaN), indium nitride (InN), and thallium nitride (TlN). This objective was achieved through Self-Consistent Field (SCF) calculations within the framework of Density Functional Theory (DFT) using the Quantum ESPRESSO package. The SCF procedure iteratively solves the Kohn–Sham equations until the total energy and electronic charge density become self-consistent, thereby ensuring that the electronic ground state is accurately described before subsequent structural, electronic, and optical calculations are performed. Quantum ESPRESSO recommends that SCF calculations satisfy a prescribed convergence threshold before any post-processing calculations, as unconverged electronic densities can propagate errors into structural optimization, band structure, density of states, and optical-property predictions.

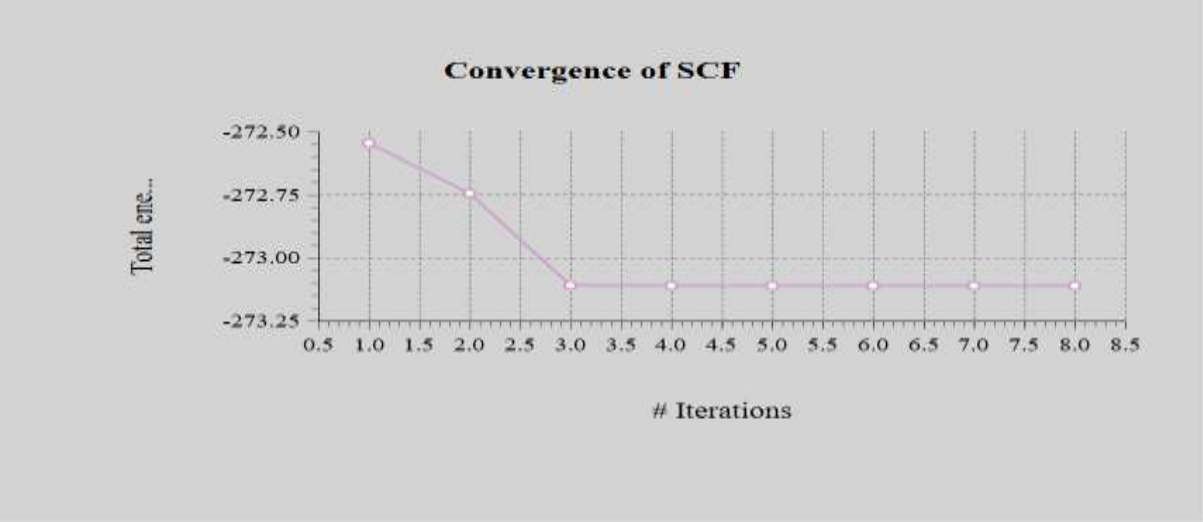

Figure 4.1: Convergence test result of TIN

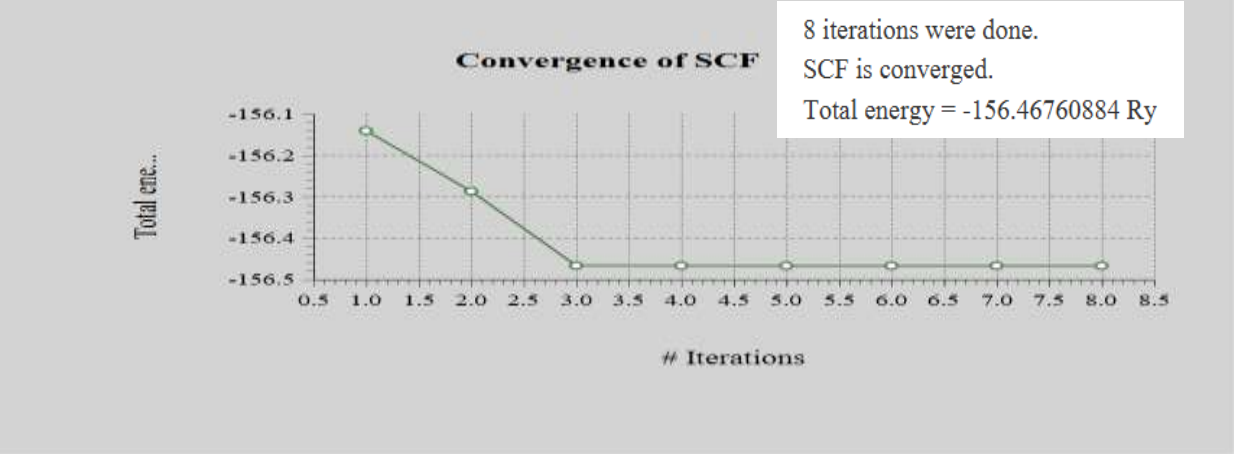

Figure 4.2: Convergence test result of InN

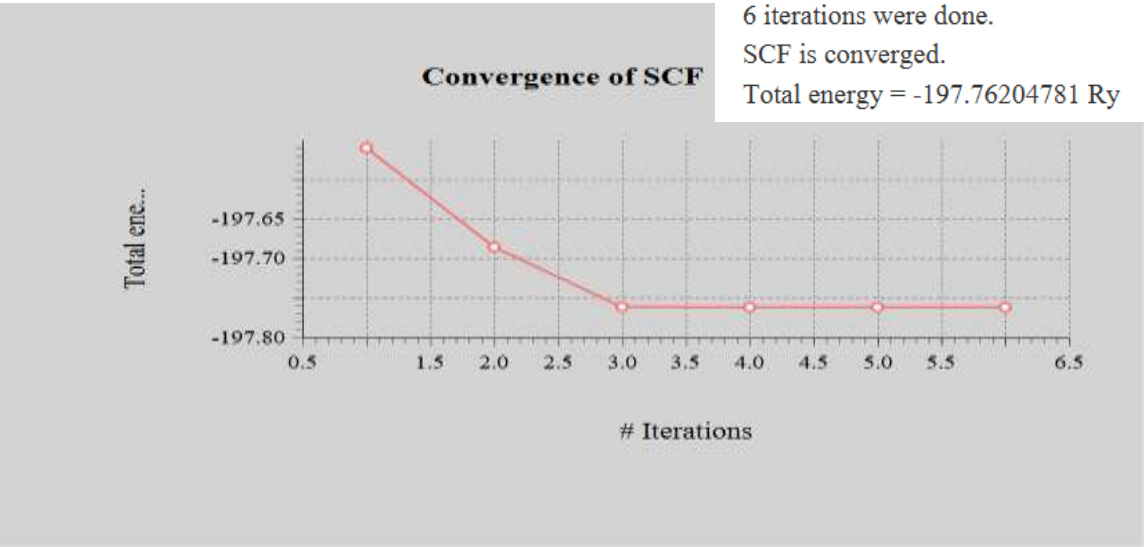

Figure 4.3: Convergence test result of GaN

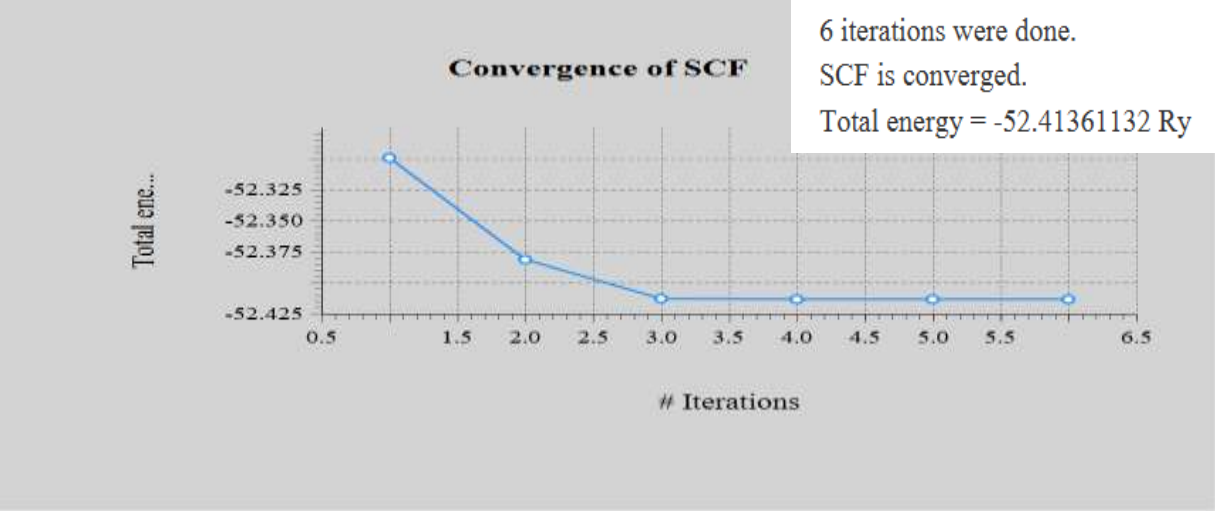

Figure 4.4: Convergence test result of BN

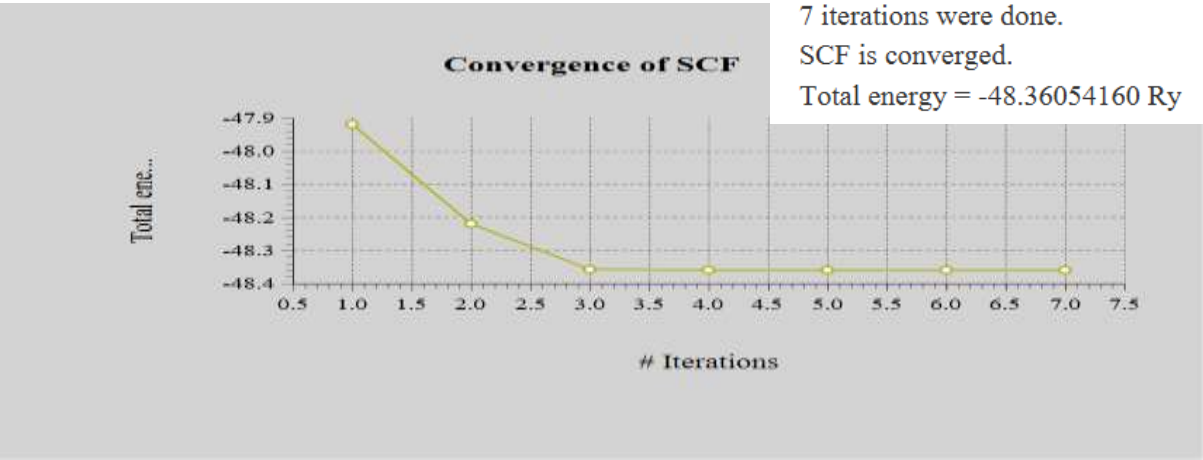

Figure 4.5: Convergence test result of AlN

Figures 4.1–4.5 illustrate the SCF convergence profiles obtained for BN, AlN, GaN, InN, and TlN, respectively. In all five compounds, the total energy decreases rapidly during the first three SCF cycles before approaching a constant value, indicating that the electronic wave functions progressively converge toward the minimum-energy solution. None of the calculations exhibited oscillatory behaviour or divergence, demonstrating that the selected computational parameters—including the exchange-correlation functional, pseudopotentials, kinetic-energy cutoff, charge-density cutoff, and Monkhorst–Pack k-point sampling—were appropriate for accurately modelling the electronic structures of the investigated nitrides.

For boron nitride (BN), the SCF calculation converged after six iterations, with a final total energy of −52.41361132 Ry. Although six SCF cycles were completed, the convergence curve indicates that the total energy stabilized after the third iteration, suggesting rapid convergence of the electronic density.

Similarly, aluminium nitride (AlN) reached convergence after seven iterations, with a final total energy of −48.36054160 Ry. The total energy remained essentially unchanged after the third iteration, indicating that the additional SCF cycles served only to satisfy the predefined electronic convergence criterion. A

similar SCF behaviour has also been reported for AlN calculations using Quantum ESPRESSO, where the energy became constant after the third iteration before reaching the specified convergence threshold.

The SCF calculation for gallium nitride (GaN) converged after six iterations, producing a final total energy of −197.76204781 Ry. As observed for BN and AlN, the energy decreased monotonically during the initial iterations and became nearly constant from the third iteration onward, indicating numerical stability throughout the calculation.

For indium nitride (InN), convergence was achieved after eight SCF iterations, with a final total energy of −156.46760884 Ry. Although InN required the largest number of iterations among the materials investigated, the convergence profile remained smooth and free from oscillations, indicating efficient electronic minimization.

Likewise, thallium nitride (TlN) converged after eight iterations, yielding a final total energy of −273.11210465 Ry. The larger number of iterations required for TlN compared with BN, AlN, and GaN may be attributed to the presence of heavier Tl atoms and stronger relativistic effects, which generally increase the complexity of electronic interactions during self-consistency. Nevertheless, the convergence remained stable, confirming the reliability of the adopted computational parameters.

Overall, the convergence behaviour observed in the present study demonstrates that all five Group 13 nitrides attained stable electronic ground states before the subsequent calculations were performed. The rapid stabilization of the total energy after approximately three SCF iterations indicates efficient charge-density mixing and a well-conditioned computational setup. Consequently, meaningful comparisons are based on the convergence methodology and computational strategy. This study is consistent with recent computational studies employing similar methodology.

Table 4.1 Comparison of the Present SCF Convergence Results for BN with Recent Studies (2022–2025)

Authors	Year	Material	DFT Package	Major Findings	Comparison with Present Study
Present Study	2026	BN, AlN, GaN, InN, TlN	Quantum ESPRESSO	The total energy decreased rapidly and stabilized after the third iteration, indicating excellent numerical stability.	Demonstrates reliable SCF convergence suitable for subsequent structural, electronic and optical property calculations.
Hasegawa et al.	2022	Wurtzite AlN	DFT (Plane-wave)	Successfully converged the SCF cycle prior to calculating lattice deformation, phase stability, and ferroelectric behaviour.	Similar to the present work, where a stable SCF solution was achieved before evaluating the material properties.
Sheng et al.	2014	Wurtzite TlN	CASTEP	Successfully achieved SCF convergence before electronic and topological analysis	Consistent with the present study in obtaining a stable ground-state solution.
Liu et al.	2024	InN	VASP	Achieved stable SCF convergence before evaluating structural and electronic properties	Consistent with the rapid convergence observed in the present study.
Camacho-García et al.	2022	GaN Surface	QE	Successfully achieved electronic self-consistency before surface-property calculations using optimized cut-off energies and k-point sampling.	Similar to the present work, where a stable SCF solution was obtained before further calculations.
Hasegawa et al.	2022	Wurtzite AlN	DFT (Plane-wave)	Successfully converged the SCF cycle prior to calculating lattice	Similar to the present work, where a stable SCF solution was achieved before

				deformation, phase stability, and ferroelectric behaviour.	evaluating the material properties.
Novotný, O., et al.	2026	BN and InN	Quantum ESPRESSO / VASP	Demonstrated that accurate prediction of III-nitride properties requires rigorous SCF convergence before structural and electronic analyses.	Supports the computational strategy adopted in the present study for obtaining reliable electronic ground-state properties.

4.2 Convergence of Plane Wave cut off-energy

Figure 4.6 presents the convergence test of the plane-wave cutoff energy for boron nitride (BN), where the calculated lattice-cell energy is plotted as a function of the plane-wave cutoff energy, ecutwfc, in Rydberg (Ry). In Quantum ESPRESSO, the plane-wave cutoff determines the size of the basis set used to represent the Kohn–Sham wavefunctions; therefore, an adequately large cutoff is required to ensure that the calculated total energy and derived structural and electronic properties are not significantly affected by the incompleteness of the basis set. Quantum ESPRESSO defines ecutwfc as the kinetic-energy cutoff for the wavefunctions, while the corresponding charge-density cutoff (ecutrho) depends on the type of pseudopotential employed.

Lattice Cell Energy Vs Plane Wave Cut-off Energy for Boron Nitride

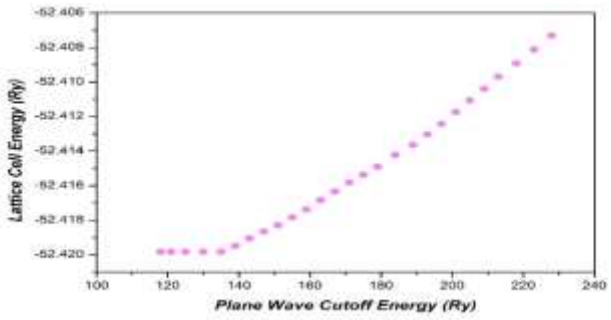

Figure 4.6: Lattice Cell Energy Vs Plane Wave Cut-off Energy for BN

Figure 4.6 shows that the lattice-cell energy of BN changes only slightly between approximately 118 and 136 Ry, remaining close to −52.420 Ry. This relatively flat region indicates that the plane-wave basis set is approaching numerical convergence, such that further increases in cutoff energy produce only minor changes in the calculated energy.

The selected cutoff is also consistent with previous first-principles studies, although direct numerical comparison should be made cautiously because cutoff requirements depend on the pseudopotential and computational setup. Mishra and Gonzalez Szwacki (2025) used a cutoff of 116 Ry with the PBE functional to investigate the structural and vibrational properties of layered BN polytypes. Similarly, Jiang et al. (2021) employed a kinetic-energy cutoff of 112 Ry for pristine and defect-containing hexagonal BN using CASTEP, PAW potentials, and the vdW-DF2 functional. These studies demonstrate that the appropriate cutoff for BN varies with the pseudopotential and exchange-correlation treatment.

Figure 4.7 presents the plane-wave cutoff-energy convergence for GaN using DFT within Quantum ESPRESSO. The cutoff energy, specified as ecutwfc, represents the maximum kinetic energy of plane waves used to expand the Kohn–Sham wavefunctions. Its proper selection is therefore essential for obtaining reliable total energies and calculated structural and electronic properties (Giannozzi et al., 2009, 2017).

Lattice Cell Energy Vs Plane Wave Cut-off Energy for Gallium Nitride

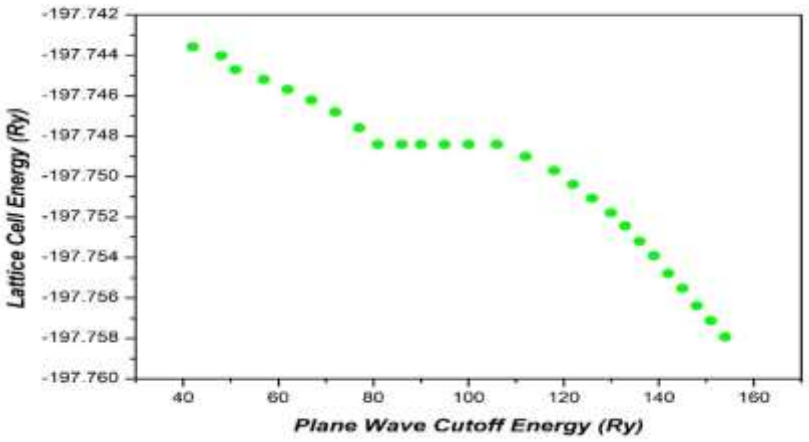

Figure 4.7: Lattice Cell Energy Vs Plane Wave Cut-off Energy for GaN

Figure 4.7 shows that the GaN lattice-cell energy decreases gradually from approximately −197.744 Ry at 42 Ry to −197.748 Ry at 80 Ry, as increasing the plane-wave cutoff improves the representation of the Kohn–Sham wavefunctions. Between approximately 80 and 105 Ry, the energy becomes nearly constant at −197.7484 Ry, indicating an apparent convergence region. However, the energy decreases further beyond about 110 Ry, reaching approximately −197.758 Ry at the highest cutoff. Therefore, the 80–105 Ry plateau should be considered a stability region rather than complete convergence unless subsequent changes fall within the predefined numerical tolerance.

The obtained behaviour is consistent with previous GaN calculations. Umari (2022) used a relatively high cutoff of 95 Ry in a Quantum ESPRESSO study of zinc-blende GaN using PBE and norm-conserving pseudopotentials. Furthermore, Prandini et al. (2018) emphasized the importance of systematic convergence testing and appropriate pseudopotential selection through the Standard Solid State Pseudopotential (SSSP) methodology, which evaluates properties such as equations of state, cohesive energies, pressure, phonon frequencies, and electronic structures.

Lattice Cell Energy Vs Plane Wave Cut-off Energy for Indium Nitride

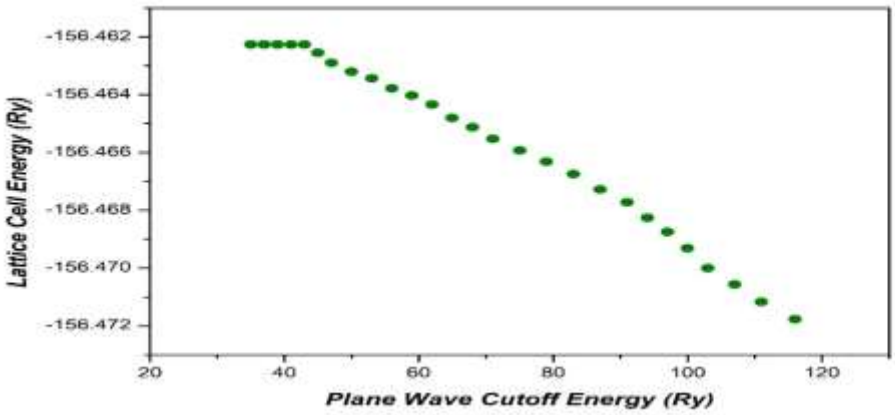

Figure 4.8: Lattice Cell Energy Vs Plane Wave Cut-off Energy for InN

Figure 4.8 presents the convergence test of the plane-wave cutoff energy for InN. The lattice-cell energy remains nearly constant between 35 and 42 Ry, at approximately −156.4623 Ry, indicating an initial stability region. However, above about 43 Ry, the energy decreases progressively, reaching approximately −156.472 Ry at 116 Ry, showing that the low-cutoff plateau does not represent complete convergence. Therefore, higher cutoff calculations are necessary to determine a reliable production value based on total-energy, force, and stress convergence criteria. Previous first-principles studies of InN have used cutoff energies ranging from approximately 30 to 100 Ry, depending on the pseudopotential and computational approach (Islam et al., 2021; Pettinari et al., 2015; Wang & Zhao, 2012).

Lattice Cell Energy Vs Plane Wave Cut-off Energy for Thallium Nitride

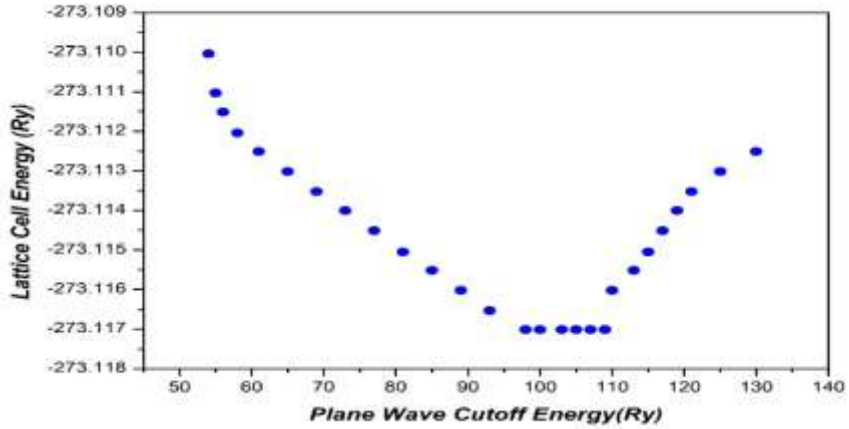

Figure 4.9: Lattice Cell Energy Vs Plane Wave Cut-off Energy for TIN

The convergence curve for TlN shows a pronounced stability region between approximately 97 and 109 Ry, where the lattice-cell energy remains nearly constant at about −273.117 Ry. The very small energy variation within this range indicates that the total energy is approaching numerical stability, making a cutoff near 100 Ry a reasonable choice for further calculations.

This result is strongly supported by Wang et al. (2012), who investigated wurtzite ($Tl_xAl_{1-x}N$) using plane-wave pseudopotential DFT with norm-conserving Troullier–Martins pseudopotentials and explicitly treated Tl 5d electrons as valence electrons. They employed a cutoff of 50 Hartree (100 Ry) for good convergence. The close agreement between their 100 Ry value and the present 97–109 Ry stability region provides an independent theoretical basis for selecting a cutoff around 100 Ry for Tl-containing nitrides using comparable pseudopotentials.

Lattice Cell Energy Vs. Plane Wave Cut off Energy for Aluminum nitride

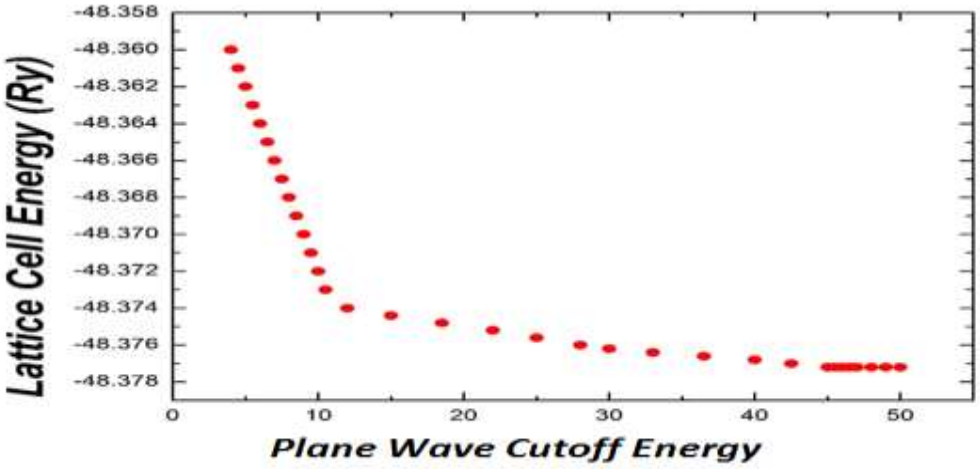

Figure 4.10: Lattice Cell Energy Vs. Plane Wave Cut off Energy for aluminum nitride

It can be seen from figures 4.10 that the lattice cell energy changes considerably with the plane wave energy cut-off, until at some energy cut-off where it becomes almost stable. In this case, as the lattice cell energy decreases, the plane wave cut off increases from 4Ry to 50Ry and becomes stable at 45Ry. That is to say, the total energy remains constant with any further increases in the plane wave energy cut-off from 45Ry. This indicates a well-converged energy cut-off. That is why 45Ry was used as the kinetic energy cut-off of the plane wave basis set for this case.

4.3 Convergence Test Results With Respect To K-Point

The k-point convergence calculations were performed to determine an adequate sampling density for integration over the Brillouin zone. Unlike the plane-wave cutoff, which controls the completeness of the basis set, the k-point mesh controls the numerical integration of electronic states throughout reciprocal space. The results for BN, AlN, GaN, InN, and TlN demonstrate that the total energy is strongly dependent on k-point sampling at low sampling densities. As the number of k-points increases, the total energy progressively approaches a region where successive calculations produce relatively small changes.

Total Energy Vs K-Point of Boron nitride

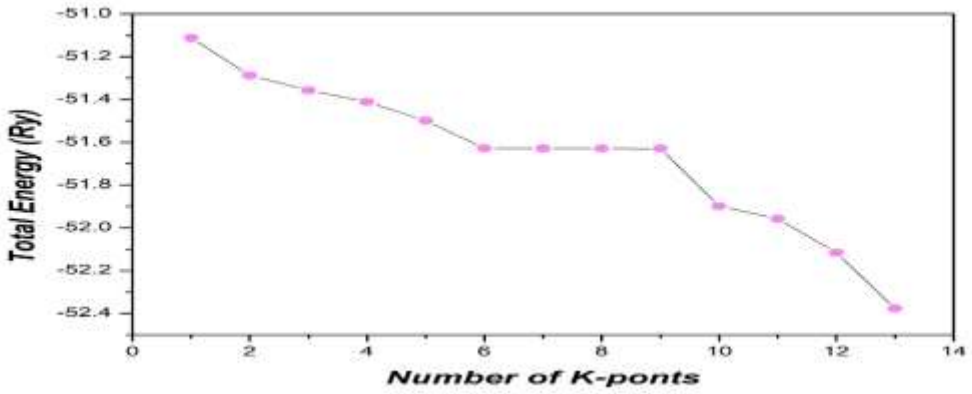

Figure 4.11: Total Energy Vs K-Point

Figure 4.11 presents the k-point convergence test for BN using Quantum ESPRESSO. The test evaluates how Brillouin-zone sampling affects the total energy, which is important for obtaining reliable total energies, charge densities, structural parameters, band structures, and density of states in periodic DFT calculations.

The BN total energy decreases from approximately −51.11 Ry at the lowest k-point sampling level to −51.50 Ry at the fifth level. Between the 6th and 9th sampling levels, the energy becomes nearly constant at approximately −51.63 Ry, indicating an apparent stability region and improved numerical convergence. Therefore, a k-point mesh within this stable range can be considered suitable, subject to the chosen numerical convergence criterion.

This behaviour is consistent with Mishra and Gonzalez Szwacki (2025), who employed a dense 16 × 16 × 16 Γ-centered Monkhorst–Pack mesh after systematic convergence testing in their first-principles study of layered BN polytypes. Their choice supports the need for sufficiently dense k-point sampling to obtain reliable BN electronic and total-energy calculations.

Total Energy Vs K-Point of Gallium nitride

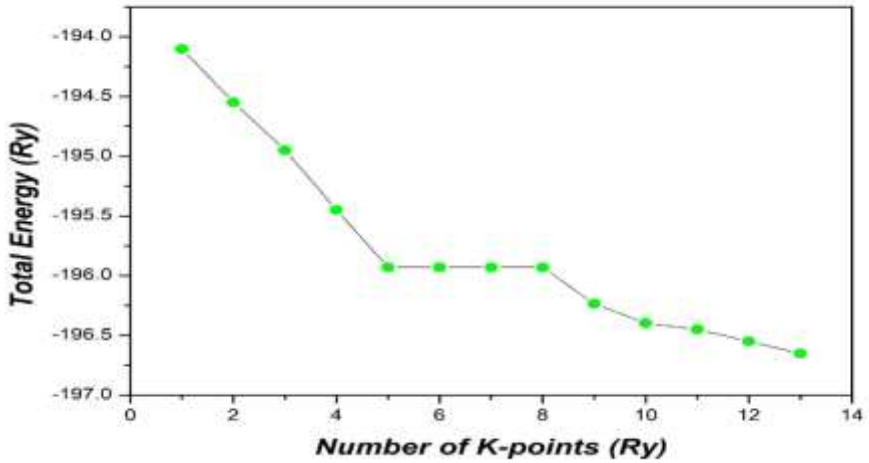

Figure 4.12: Total Energy Vs K-Point

Figure 4.12 presents the k-point convergence test for GaN. The total energy decreases substantially from approximately −194.10 Ry at the first sampling level to −195.93 Ry at the fifth, indicating that the initial k-point meshes are insufficient for accurate Brillouin-zone integration. An apparent stability region occurs between the 5th and 8th sampling levels, where the energy remains close to −195.93 Ry. However, the subsequent decrease to approximately −196.65 Ry at the 13th level demonstrates that this plateau does not represent complete convergence. Therefore, further k-point testing is required, with the final mesh selected using a quantitative energy-convergence tolerance rather than visual inspection alone.

The observed trend agrees with previous GaN studies. Qin et al. (2017) used a 12 × 12 × 12 Monkhorst–Pack mesh after convergence testing, achieving an energy variation below 1 meV atom^{-1}. Zhang (2023) reported that a 9 × 9 × 9 grid converged the bulk GaN lattice parameter within 0.001 Å, while Lu et al. (2019) employed a denser 18 × 18 × 1 mesh for bilayer GaN. These studies support the importance of progressively denser k-point sampling for reliable GaN calculations.

Total Energy Vs K-Point of Indium nitride

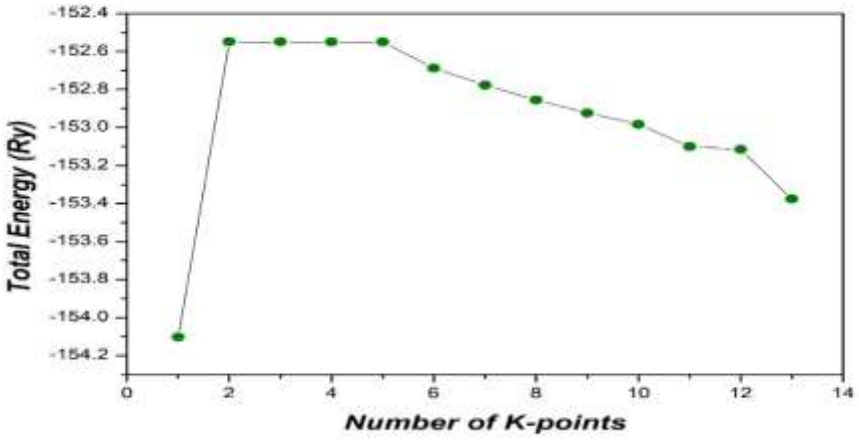

Figure 4.13: Total Energy Vs K-Point

Figure 4.13 presents the k-point convergence test for InN. The total energy varies significantly at low sampling densities, changing from approximately −154.10 Ry at the first level to −152.55 Ry at the second level, followed by an apparent stability region between the 2nd and 5th sampling levels. However, the energy decreases progressively from the 6th level onward, reaching approximately −153.37 Ry at the highest sampling level. This continued variation indicates that the intermediate plateau does not represent complete convergence and that denser Brillouin-zone sampling is required for reliable InN calculations.
The observed behaviour is consistent with previous first-principles studies of wurtzite InN, which have used k-point meshes ranging from 8 × 8 × 4 to 12 × 12 × 6, with more demanding electronic-structure calculations employing meshes as dense as 16 × 16 × 12. These results support the need for adequate reciprocal-space sampling. Nevertheless, because the total energy continues to change at the highest sampling level, further convergence testing is recommended, with the final mesh determined using a quantitative energy-convergence criterion rather than visual inspection alone.

Total Energy Vs K-Point of Thallium nitride

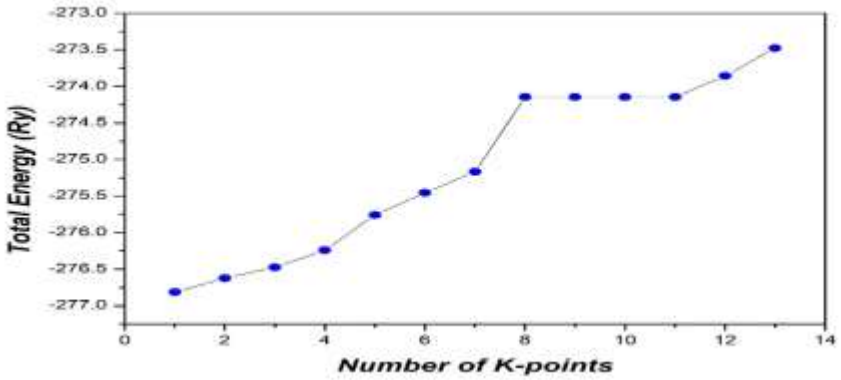

Figure 4.14: Total Energy Vs K-Point

Figure 4.14 presents the k-point convergence test for TlN. The total energy varies considerably at low sampling densities, changing from approximately −276.82 Ry at the first level to −275.17 Ry at the seventh level (6 × 6 × 2). A further significant change occurs at the eighth level (8 × 8 × 1), after which the energy remains nearly constant at approximately −274.14 Ry up to the eleventh level (10 × 10 × 2). This plateau represents an apparent convergence region. However, the subsequent increase in energy to approximately −273.85 Ry and −273.48 Ry at the 12th and 13th levels indicates that complete convergence has not yet been achieved.

Previous studies support the use of moderately dense to dense k-point meshes for TlN. Ferhat and Zaoui (2006) used an 8 × 8 × 4 Monkhorst–Pack mesh, achieving approximately 1 mRy per unit cell accuracy, while Saidi-Houat et al. (2007) employed 9 × 9 × 4. Sheng et al. (2014) used a denser 13 × 13 × 7 mesh to study the electronic and topological properties of TlN. These studies broadly support the present convergence behaviour. Nevertheless, because the total energy changes at the highest sampling levels, the final k-point mesh should be determined using a quantitative energy-convergence criterion rather than the apparent plateau alone. This is especially relevant for TlN because the heavy Tl atom can make relativistic and spin–orbit effects important in its electronic structure.

The convergence test results with respect to the kinetic energy cut-off and k-points for the Aluminium nitride is presented below.

Total Energy Vs K-Point

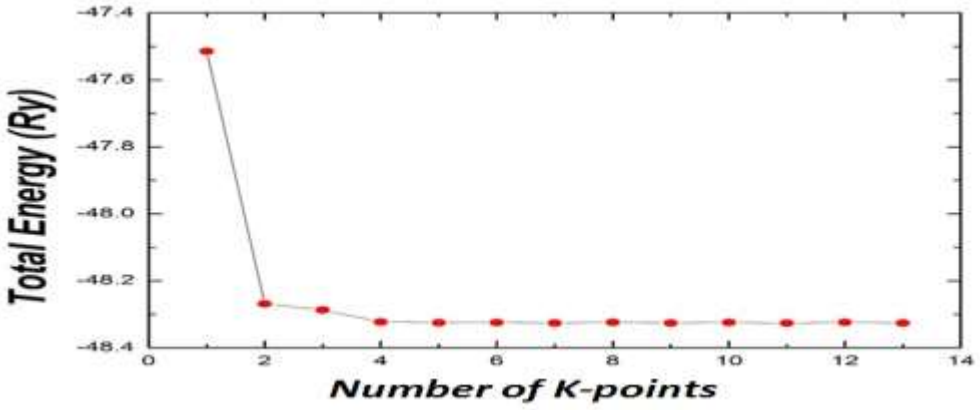

Figure 4.15: Total Energy Vs K-Point

Figures 4.15 shows the variations of the total energy with respect to the k-points grids. The total energy becomes independent of the number of k-points at a certain points, showing a well-converged value at -48.3227 RY. The total energy keeps changing from 1×1×0 to 4×4×1 k-point grids and then it almost becomes stable from 4×4×2 k-points which is indicating a converged value. As such, 4×4×2 k-points have been adopted for this case. Furthermore, Monkhorst and Pack method of selecting k-points is commonly used in most DFT calculations Monkhorst H. and Pack, J. [1976]. Most of the DFT codes provide ways of choosing k-points using Monkhorst and Pack method. So, one of the basic idea adopted in the method is to specify the number of k-points that are to be used in each direction in reciprocal space.

4.4 Lattice Parameter

The equilibrium lattice parameters of BN, AlN, GaN, InN, and TlN were determined using first-principles calculations in Quantum ESPRESSO by systematically varying the lattice parameter and calculating the corresponding total energy. The equilibrium lattice parameter was identified from the minimum of the total-energy curve, representing the most stable crystal configuration at zero pressure.

Overall, the results show that the lattice parameter strongly influences the structural stability of the Group-13 nitrides. As the lattice parameter approaches its equilibrium value, the total energy decreases because the interatomic distances become energetically favorable. Deviations from this value, through

either expansion or contraction, increase the total energy by disturbing the balance between attractive bonding and short-range repulsive interactions. Thus, the minimum-energy position provides the appropriate equilibrium lattice parameter for each material and forms the basis for subsequent electronic and optical-property calculations.

Crystal Cell Energy Vs. Lattice Parameter for Boron nitride

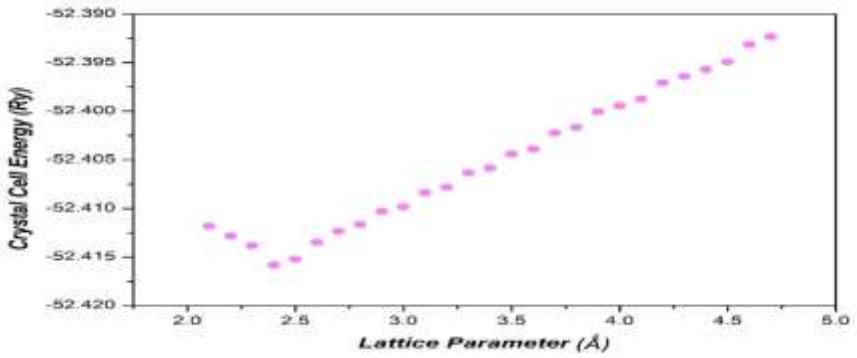

Figure 4.16: Lattice parameter for BN

Figure 4.16 shows the variation of BN crystal-cell energy with lattice parameter calculated using DFT in Quantum ESPRESSO. The equilibrium lattice parameter is determined from the point of minimum total energy, which represents the most stable crystal configuration.

The calculated curve exhibits a clear U-shaped behaviour, with the energy decreasing as the lattice parameter increases and reaching a minimum of approximately −52.416 Ry at a≈2.40 Å. Beyond this point, the energy increases with further lattice expansion, confirming the presence of a stable equilibrium structure.

For comparison, Novotný et al. (2024) reported an experimental in-plane lattice constant of approximately 2.5058 Å for bulk hexagonal BN (h-BN). They also noted that h-BN presents challenges for conventional DFT because of the combination of strong in-plane covalent bonding and relatively weak interlayer van der Waals interactions. Thus, the present calculated value of 2.40 Å is somewhat smaller than the experimental value, indicating a difference of approximately 0.106 Å, which may be associated with the computational method and treatment of interlayer interactions.

Crystal Cell Energy Vs. Lattice Parameter for Gallium nitride

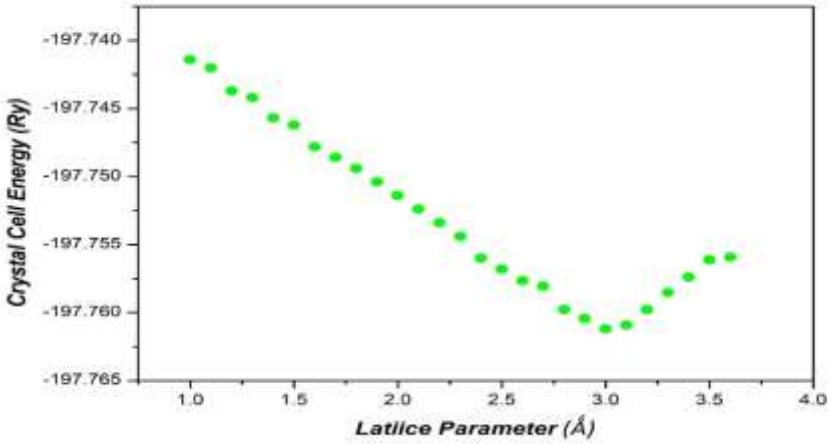

Figure 4.17: Lattice parameter for GaN

The GaN total-energy curve shows that the energy decreases as the lattice parameter increases from approximately 1.0 Å, reaching a minimum of about −197.762 Ry at 3.09 Å. Beyond this point, the energy increases gradually, indicating that further lattice expansion is energetically unfavourable. Thus, the calculated equilibrium lattice parameter of GaN is approximately 3.09 Å.
This determination is consistent with the standard DFT approach in which the equilibrium lattice constant corresponds to the minimum of the total-energy curve, as implemented in Quantum ESPRESSO (Giannozzi et al., 2009, 2017). However, the calculated value is somehow smaller than the experimental lattice parameter of approximately 3.189 Å reported for stable bulk wurtzite GaN (Paszkowicz et al., 2004; Chen et al., 2024). In comparison, Chen et al. (2024) obtained a PBE value of approximately 3.23 Å, while Bouhassoune et al. (2017) reported a GGA value of 3.242 Å, both showing reasonable agreement with experiment.

Crystal Cell Energy Vs. Lattice Parameter for Indium nitride

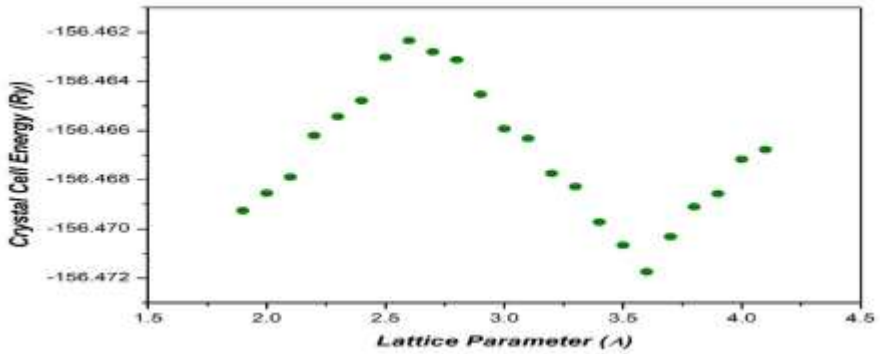

Figure 4.18: Lattice parameter for InN

The InN total-energy curve shows a decrease in energy as the lattice parameter increases from approximately 1.9 Å, reaching a minimum of about −156.4718 Ry at 3.60 Å. Beyond this point, the

energy increases with further expansion, confirming that 3.60 Å represents the calculated equilibrium lattice parameter.

The calculated value is slightly larger than the experimental value of approximately 3.54 Å, corresponding to a deviation of about 1.55%. Nevertheless, it agrees well with previous PBE-based theoretical values of 3.58–3.62 Å reported by Liang et al. (2017) and Arellano-Ramírez et al. (2026). The slight overestimation is consistent with the tendency of PBE-type functionals to predict somewhat larger lattice parameters. Differences obtained using PBEsol and WC further demonstrate that the choice of exchange-correlation functional and pseudopotential can influence the predicted equilibrium structure.

Crystal Cell Energy Vs. Lattice Parameter for Thallium nitride

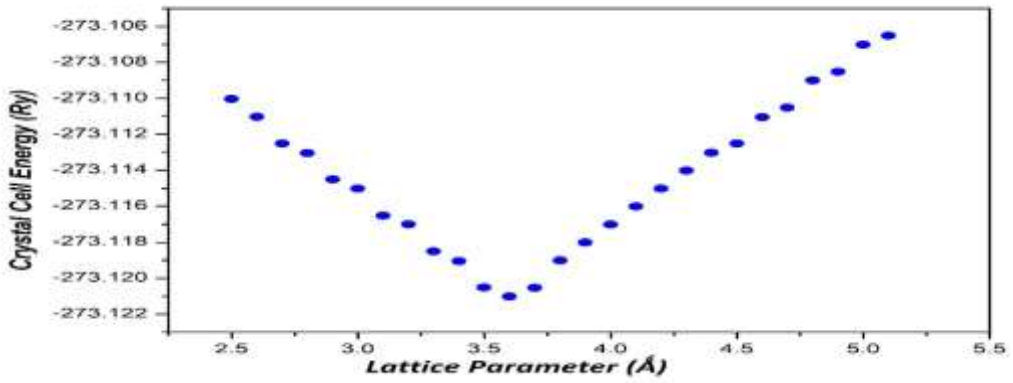

Figure 4.19: Lattice parameter for TIN

Figure 4.19 presents the calculated crystal-cell energy of wurtzite TlN as a function of lattice parameter. The energy decreases as the lattice parameter increases from approximately 2.5 Å, reaching a minimum of about −273.121 Ry at a≈3.615 Å. Beyond this point, the energy increases continuously, indicating that further lattice expansion is energetically unfavorable. Thus, 3.615 Å is identified as the equilibrium lattice parameter of TlN from the present calculation.

The calculated value is reasonably consistent with previous theoretical results. Farzan et al. (2016) reported wurtzite TlN lattice parameters ranging from 3.6461 Å (LDA) to 3.7398 Å (GGA-PBE), while PBEsol and Wu–Cohen yielded 3.6806 Å and 3.6840 Å, respectively. The present value of 3.615 Å is therefore slightly lower but remains within the range of previously reported theoretical predictions.

Crystal Cell Energy Vs. Lattice Parameter for Aluminum nitride

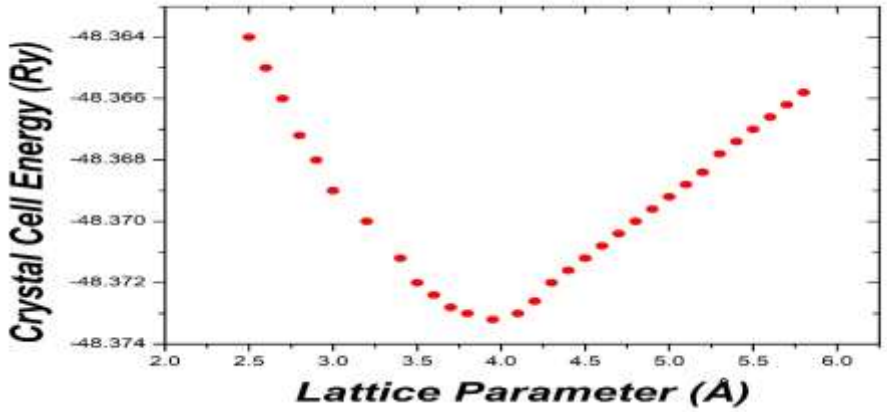

Figure 4.20: Lattice parameter for Aluminum nitride

The equilibrium value of the lattice parameter *a*obtained at the point of minimum energy is about 3.95 Å. The result obtained in this research were in good agreement with other computational work by worksof Javaheri et al., [2016],Maziar et al., [2018], Giovanne et al., [2019],Sake et al., [2019] and Hamad R. and Magged A. [2014]. Thus, the present studies also have a good agreement with the experimental value. Experimentally the lattice parameter of AlN is 4.37 Å Edgar, J. [1994]. The deviation of result as shown in figure 4.5 from the experimental result is about 0.42Å of absolute error which is equivalent to 9.6% of relative error.

CONCLUSION AND RECOMMENDATION

The study used Density Functional Theory (DFT) in the Quantum ESPRESSO framework to investigate the convergence and structural properties of BN, AlN, GaN, InN, and TlN**,** using the PBE-GGA functional, ultrasoft pseudopotentials, plane-wave basis sets, and Monkhorst–Pack k-point sampling. The SCF calculations showed stable convergence for all materials, with BN, AlN, and GaN converging in 6, 7, and 6 iterations, respectively, while InN and TlN required 8 iterations. TlN converged more slowly, likely because of the heavy Tl atom and stronger relativistic effects. Cutoff-energy tests revealed material-dependent convergence. Stable regions were observed around 118–136 Ry for BN, 80–105 Ry for GaN, 97–109 Ry for TlN, and approximately 45 Ry for AlN. InN required further testing because its total energy continued decreasing at higher cutoff energies. The k-point tests also demonstrated that Brillouin-zone sampling influences total-energy accuracy. While some materials displayed apparent stability regions, BN, GaN, InN, and TlN showed further changes at higher sampling densities. For AlN, a 4 × 4 × 2 mesh was selected after the energy became approximately constant at −48.3227 Ry. Structural optimization produced equilibrium lattice parameters of approximately 2.40 Å (BN), 3.95 Å (AlN), 3.09 Å (GaN), 3.60 Å (InN), and 3.615 Å (TlN)**.** Comparison with previous theoretical and experimental studies showed generally reasonable agreement, particularly for InN. Overall, the findings demonstrate that systematic cutoff-energy and k-point convergence testing is essential for reliable DFT calculations**, while** total-energy minimization provides an effective approach for determining equilibrium lattice parameters**.**

It is recommended that further quantitative convergence testing be carried out, particularly for InN, GaN, and TlN, using well-defined numerical tolerances for cutoff energy and k-point sampling. Future studies should also employ advanced exchange-correlation methods, such as hybrid functionals and GW/BSE approaches, to improve the accuracy of electronic and optical-property predictions. The optimized structures obtained in this study should be used for detailed investigations of band structures, density of states, band gaps, and optical properties. In addition, the effects of strain, pressure, temperature, defects, and doping should be examined, while further experimental studies—especially for TlN—are encouraged to validate the theoretical results. These efforts will enhance the reliability of the calculations and support the potential application of Group 13 nitrides in optoelectronic and photovoltaic technologies.

REFERENCES

Ali, A., & Reshak, A. H. (2010). Anisotropic optical properties of wurtzite InN from *ab initio* calculations. *Journal of Physics and Chemistry of Solids, 71*(3), 403–408. https://doi.org/10.1016/j.jpcs.2009.11.004

Amano, H., et al. (2018). The 2018 GaN power electronics roadmap. *Journal of Physics D: Applied Physics, 51*(16), 163001.

Ambacher, O. (1998). Growth and applications of group III-nitrides. *Journal of Physics: Condensed Matter, 10*(32), 7131.

As, D. J., et al. (1997). Optical and structural properties of epitaxial AlN layers grown on 6H-SiC. *Applied Physics Letters, 70*(10), 1311–1313. https://doi.org/10.1063/1.118544

Bechstedt, F., Furthmüller, J., & Wimmer, E. (2002). *Ab initio* studies of InN polymorphs: Band gaps and crystal-field splitting. *Journal of Applied Physics, 92*(11), 6416–6422. https://doi.org/10.1063/1.1515114

Blase, X., Rubio, A., Louie, S. G., & Cohen, M. L. (1995). Quasiparticle band structure of bulk hexagonal boron nitride and related systems. *Physical Review B, 51*(11), 6868–6875. https://doi.org/10.1103/PhysRevB.51.6868

Brandt, O., et al. (2004). The synthesis of high-quality InN films by molecular beam epitaxy. *Journal of Crystal Growth, 272*(1–4), 242–250.

Breternitz, J., & Schorr, S. (2021). Symmetry relations in wurtzite nitrides and oxide nitrides and the curious case of $Pmc2_1$. *Acta Crystallographica Section A: Foundations and Advances, 77*(3), 208–216. https://doi.org/10.1107/S2053273320015971

Cassabois, G., Valvin, P., & Gil, B. (2016). Hexagonal boron nitride is an indirect bandgap semiconductor. *Nature Photonics, 10*(4), 262–266. https://doi.org/10.1038/nphoton.2015.277

Cheng, Y., Zhu, Y., Liu, Y., & Xie, M. (2018). Hexagonal boron nitride: Synthesis, properties and applications. *Materials Chemistry and Physics, 223*, 372–387. https://doi.org/10.1016/j.matchemphys.2018.11.033

Christensen, N. E., & Gorczyca, I. (1994). Optical and structural properties of III–V nitrides under pressure. *Physical Review B, 50*(7), 4397–4415.

Davydov, V. Y., et al. (1998). Absorption and emission of hexagonal GaN and AlN. *Journal of Applied Physics, 82*(10), 5097–5108. https://doi.org/10.1063/1.366492

Davydov, V. Y., et al. (2002). Absorption and photoluminescence of hexagonal InN. *Physica Status Solidi (B), 229*(3), R1–R3. https://doi.org/10.1002/1521-3951(200201)229:3R1::AID-PSSB999913.0.CO;2-V

Farvacque, J.-L., Bougrioua, Z., Vennéguès, P., & Monroy, E. (2005). Optical constants of InN thin films. *Applied Physics Letters, 87*(6), 061103. https://doi.org/10.1063/1.2009814

Farzan, M., Elahi, S. M., Salehi, H., & Abolhassani, M. R. (2016). A comparison of the structural, electronic, optical and elastic properties of wurtzite, zinc-blende and rock salt TlN: A DFT study. *Acta Physica Polonica A, 130*(3), 758–768. https://doi.org/10.12693/APhysPolA.130.758

Feneberg, M., Leute, R. A. R., Neuschl, B., et al. (2010). High-excitation and high-resolution photoluminescence spectra of bulk AlN.

Ferhat, M., & Zaoui, A. (2006). Do all III–V compounds have the zinc-blende or wurtzite ground-state structure? *Applied Physics Letters, 88*(16), 161902. https://doi.org/10.1063/1.2196050

Giannozzi, P., Baroni, S., Bonini, N., Calandra, M., Car, R., Cavazzoni, C., Ceresoli, D., Chiarotti, G. L., Cococcioni, M., Dabo, I., Dal Corso, A., de Gironcoli, S., Delugas, P., DiStasio, R. A., Jr., Ferretti, A., Fratesi, G., Gerstmann, U., Gougoussis, C., Kokalj, A., Lazzeri, M., Martin-Samos, L., Marzari, N., Mauri, F., Mazzarello, R., Paolini, S., Pasquarello, A., Paulatto, L., Sbraccia, C., Scandolo, S., & Wentzcovitch, R. M. (2009). Quantum ESPRESSO: A modular and open-source software project for quantum simulations of materials. *Journal of Physics: Condensed Matter, 21*(39), 395502. https://doi.org/10.1088/0953-8984/21/39/395502

Giannozzi, P., Andreussi, O., Brumme, T., Bunau, O., Buongiorno Nardelli, M., Calandra, M., Car, R., Cavazzoni, C., Ceresoli, D., Cococcioni, M., Colonna, N., Carnimeo, I., Dal Corso, A., de Gironcoli, S., Delugas, P., DiStasio, R. A., Jr., Ferretti, A., Floris, A., Fratesi, G., et al. (2017). Advanced capabilities for materials modelling with Quantum ESPRESSO. *Journal of Physics: Condensed Matter, 29*(46), 465901. https://doi.org/10.1088/1361-648X/aa8f79

Golenić, D., et al. (2024). Optically driven plasmons in graphene/hBN van der Waals heterostructures: Simulating s-SNOM measurements. *Nanophotonics*. https://doi.org/10.1515/nanoph-2023-0841

Hohenberg, P., & Kohn, W. (1964). Inhomogeneous electron gas. *Physical Review, 136*(3B), B864–B871.

Hoffmann, A., et al. (2001). Optical properties of AlN single crystals and epitaxial layers. *Physica Status Solidi (B), 228*(1), 215–218. https://doi.org/10.1002/1521-3951(200105)228:1<215::AID-PSSB215>3.0.CO;2-L

Hybertsen, M. S., & Louie, S. G. (1986). Electron correlation in semiconductors and insulators: Band gaps and quasiparticle energies. *Physical Review B, 34*(8), 5390–5413. https://doi.org/10.1103/PhysRevB.34.5390

International Renewable Energy Agency. (2020). *Solar energy: A key pillar of the global energy transformation*.

Islam, M. S., Zamil, M. Y., Mojumder, M. R. H., Stampfl, C., Park, J., et al. (2021). Strong tribo-piezoelectric effect in bilayer indium nitride (InN). *Scientific Reports, 11*, 18669. https://doi.org/10.1038/s41598-021-98130-5

Jain, S. C., Willander, M., Narayan, J., & Van Overstraeten, R. (2000). III–nitrides: Growth, characterization, and properties. *Journal of Applied Physics, 87*(3), 965–1006. https://doi.org/10.1063/1.371971

Jiang, H. X., Lin, J. Y., & Khan, M. A. (2004). Optical and electronic properties of InN and related compounds. *Applied Physics Letters, 85*(14), 2624–2626. https://doi.org/10.1063/1.1794866

Jiang, T., Le, D., Rawal, T. B., & Rahman, T. S. (2021). Syngas molecules as probes for defects in 2D hexagonal boron nitride: Their adsorption and vibrations. *Physical Chemistry Chemical Physics, 23*, 7988–8001.

Kabir, E., Kumar, P., Kumar, S., Adelodun, A. A., & Kim, K.-H. (2018). Solar energy: Potential and future prospects. *Renewable and Sustainable Energy Reviews, 82*, 894–900. https://doi.org/10.1016/j.rser.2017.09.094

Kohn, W., & Sham, L. J. (1965). Self-consistent equations including exchange and correlation effects. *Physical Review, 140*(4A), A1133–A1138. https://doi.org/10.1103/PhysRev.140.A1133

Kresse, G., & Furthmüller, J. (1996a). Efficiency of *ab initio* total energy calculations for metals and semiconductors using a plane-wave basis set. *Computational Materials Science, 6*(1), 15–50.

Kresse, G., & Furthmüller, J. (1996b). Efficient iterative schemes for *ab initio* total-energy calculations using a plane-wave basis set. *Physical Review B, 54*(16), 11169–11186.

Lambrecht, W. R. L., Segall, B., & Rashkeev, S. N. (2000). Optical properties of GaN. *Physical Review B, 62*(4), 2569–2577. https://doi.org/10.1103/PhysRevB.62.2569

Li, X., et al. (2020). Density functional theory study of the structural, electronic, and optical properties of BN nanotubes. *Physical Review B, 101*(11), 115405.

Liu, C., Liu, G., et al. (2014). Single-crystalline GaN nanotube arrays grown on Al_2O_3 substrates using InN nanorods as templates. *Journal of Crystal Growth, 389*, 1–4. https://doi.org/10.1016/j.jcrysgro.2013.11.066

Lu, D., Schilfgaarde, M. V., & Kotani, T. (2006). Quasiparticle calculations of the electronic properties of wurtzite InN and GaN. *Physical Review B, 74*(19), 195104. https://doi.org/10.1103/PhysRevB.74.195104

Lu, H., Schaff, W. J., Eastman, L. F., & Wu, J. (2002). Low band gap of InN. *Journal of Crystal Growth, 227–228*, 466–469. https://doi.org/10.1016/S0022-0248(01)01041-6

Lu, A. K. A., Yayama, T., Morishita, T., Spencer, M. J. S., & Nakanishi, T. (2019). Uncovering new buckled structures of bilayer GaN: A first-principles study. *The Journal of Physical Chemistry C, 123*(3), 1939–1947. https://doi.org/10.1021/acs.jpcc.8b09973

Marini, A., Hogan, C., Grüning, M., & Varsano, D. (2009). Yambo: An *ab initio* tool for excited state calculations. *Computer Physics Communications, 180*(8), 1392–1403. https://doi.org/10.1016/j.cpc.2009.02.003

Martin, R. M. (2004). *Electronic structure: Basic theory and practical methods*. Cambridge University Press.

Martin, R. M. (2020). *Electronic structure: Basic theory and practical methods* (2nd ed.). Cambridge University Press.

Mishra, P., & Gonzalez Szwacki, N. (2025). Raman and infrared signatures of layered boron nitride polytypes: A first-principles study. *Nanomaterials, 15*(20), 1567. https://doi.org/10.3390/nano15201567

Monemar, B. (1974). Fundamental energy gap of GaN from photoluminescence excitation spectra. *Physical Review B, 10*(2), 676–681. https://doi.org/10.1103/PhysRevB.10.676

Monkhorst, H. J., & Pack, J. D. (1976). Special points for Brillouin-zone integrations. *Physical Review B, 13*(12), 5188–5192. https://doi.org/10.1103/PhysRevB.13.5188

Morkoç, H. (2009). *Handbook of nitride semiconductors and devices: Materials properties, physics and growth* (Vol. 1). Wiley-VCH.

Moses, P. G., Miao, M., Yan, Q., & Van de Walle, C. G. (2011). Hybrid functional investigations of band gaps and band alignments for AlN, GaN, InN, and InGaN. *The Journal of Chemical Physics, 134*(8), 084703. https://doi.org/10.1063/1.3553714

Neugebauer, J., & Van de Walle, C. G. (1994). Gallium vacancies and the yellow luminescence in GaN. *Applied Physics Letters, 64*(6), 728–730. https://doi.org/10.1063/1.111434

Noei, M., Salari, A. A., Ahmadaghaei, N., et al. (2013). DFT study of the dissociative adsorption of HF on an AlN nanotube. *Comptes Rendus Chimie, 16*, 985–989. https://doi.org/10.1016/j.crci.2013.05.007

Novotný, J., Dubecký, M., & Karlický, F. (2024). Toward accurate modeling of structure and energetics of bulk hexagonal boron nitride. *Journal of Computational Chemistry*. https://doi.org/10.1002/jcc.27222

Onida, G., Reining, L., & Rubio, A. (2002). Electronic excitations: Density-functional versus many-body Green's-function approaches. *Reviews of Modern Physics, 74*(2), 601–659. https://doi.org/10.1103/RevModPhys.74.601

Pakdel, A., Bando, Y., & Golberg, D. (2014). Nano boron nitride flatland. *Chemical Society Reviews, 43*(3), 934–959.

Pankove, J. I., & Hutchby, J. A. (1975). Optical properties of GaN. *Journal of Applied Physics, 46*(8), 3333–3336. https://doi.org/10.1063/1.321866

Paszkowicz, W., Podsiadło, S., & Minikayev, R. (2004). Rietveld-refinement study of aluminium and gallium nitrides. *Journal of Alloys and Compounds, 382*(1–2), 100–106. https://doi.org/10.1016/j.jallcom.2004.05.036

Pettinari, G., Filippone, F., Polimeni, A., Mattioli, G., Patanè, A., Lebedev, V., Capizzi, M., & Amore Bonapasta, A. (2015). Genesis of "solitary cations" induced by atomic hydrogen. *Advanced Functional Materials, 25*(33), 5353–5359. https://doi.org/10.1002/adfm.201501858

Perdew, J. P., Burke, K., & Ernzerhof, M. (1996). Generalized gradient approximation made simple. *Physical Review Letters, 77*(18), 3865–3868. https://doi.org/10.1103/PhysRevLett.77.3865

Ponce, F. A., & Bour, D. P. (1997). Nitride-based semiconductors for blue and green light-emitting devices. *Nature, 386*(6623), 351–359. https://doi.org/10.1038/386351a0

Prandini, G., Marrazzo, A., Castelli, I. E., Mounet, N., & Marzari, N. (2018). Precision and efficiency in solid-state pseudopotential calculations. *npj Computational Materials, 4*, 72. https://doi.org/10.1038/s41524-018-0127-2

Ribeiro, R. M., & de Castro, A. S. (2006). Electronic properties of hexagonal boron nitride monolayers. *Physical Review B, 74*(4), 045406. https://doi.org/10.1103/PhysRevB.74.045406

Rinke, P., Janotti, A., Scheffler, M., & Van de Walle, C. G. (2008). Band gap and band parameters of GaN from quasiparticle energy calculations based on exact-exchange density-functional theory. *Physical Review B, 77*(7), 075202. https://doi.org/10.1103/PhysRevB.77.075202

Sachs, B., Wehling, T. O., Katsnelson, M. I., & Lichtenstein, A. I. (2011). Adhesion and electronic structure of graphene on hexagonal boron nitride substrates. *Physical Review B, 84*(19), 195414. https://doi.org/10.1103/PhysRevB.84.195414

Saidi-Houat, N., Zaoui, A., & Ferhat, M. (2007). Structural stability of thallium–V compounds. *Journal of Physics: Condensed Matter, 19*(10), 106221. https://doi.org/10.1088/0953-8984/19/10/106221

Sahin, H., et al. (2009). Monolayer honeycomb structures of group-IV elements and III–V binary compounds: First-principles calculations. *Physical Review B, 80*(15), 155453.

Schaff, W. J., Eastman, L. F., & Smart, J. A. (2002). Growth and characterization of InN thin films. *Journal of Crystal Growth, 248*(1–4), 557–562. https://doi.org/10.1016/S0022-0248(02)01970-2

Sheng, X.-L., Wang, Z., Yu, R., Weng, H., Fang, Z., & Dai, X. (2014). Topological insulator to Dirac semimetal transition driven by sign change of spin–orbit coupling in thallium nitride. *Physical Review B, 90*(24), 245308. https://doi.org/10.1103/PhysRevB.90.245308

Shishkin, M., & Kresse, G. (2007). Self-consistent GW calculations for semiconductors and insulators. *Physical Review B, 75*(23), 235102.

Singh, A. K., Kumar, P., & Yadav, R. N. (2021). First-principles study of electronic and optical properties of group III nitrides using DFT. *Materials Today: Proceedings, 46*, 2466–2470. https://doi.org/10.1016/j.matpr.2020.11.364

Slack, G. A. (1973). Nonmetallic crystals with high thermal conductivity. *Journal of Physics and Chemistry of Solids, 34*(2), 321–335. https://doi.org/10.1016/S0022-3697(73)80291-9

Slack, G. A., & McNelly, T. F. (1973). Growth of high-purity AlN crystals. *Journal of Crystal Growth, 34*(2), 263–279. https://doi.org/10.1016/0022-0248(73)90161-6

Solozhenko, V. L., Lazarenko, A. G., Petitet, J. P., & Kanaev, A. V. (2001). Bandgap energy of graphite-like hexagonal boron nitride. *Journal of Applied Physics, 89*(11), 5777–5779. https://doi.org/10.1063/1.1354656

Stampfl, C., & Van de Walle, C. G. (2002). Density-functional calculations for III–V nitrides using the local-density approximation and the generalized gradient approximation. *Physical Review B, 65*(15), 155212.

Strak, P., Gorczyca, I., & Teisseyre, H. (2024). Bandgap characteristics of boron-containing nitrides—*Ab initio* study for optoelectronic applications. *Materials, 17*(20), 5120. https://doi.org/10.3390/ma17205120

Strak, P., Sakowski, K., Kempisty, P., Grzegory, I., Kaminska, A., & Krukowski, S. (2025). *Ab initio* elucidation of the nature of the bonding of tetrahedral nitrides (BN, AlN, GaN, and InN), hexagonal BN, and graphene. *Materials, 18*(12), 2875. https://doi.org/10.3390/ma18122875

Taniyasu, Y., Kasu, M., & Makimoto, T. (2006). An aluminium nitride light-emitting diode with a wavelength of 210 nanometres. *Nature, 441*(7091), 325–328. https://doi.org/10.1038/nature04759

Tansley, T. L., & Foley, C. P. (1996). Optical band gap of indium nitride. *Journal of Applied Physics, 59*(9), 3241–3244.

Ueda, T., Tanaka, T., & Uesugi, T. (2014). GaN power devices: Current status and future prospects. *Japanese Journal of Applied Physics, 53*(10), 100214. https://doi.org/10.7567/JJAP.53.100214

Van de Walle, C. G., & Neugebauer, J. (2004). First-principles calculations for defects and impurities: Applications to III-nitrides. *Journal of Applied Physics, 95*(8), 3851–3879. https://doi.org/10.1063/1.1682673

Wang, S., et al. (2019). First-principles study of the structural, electronic, and optical properties of AlN, GaN, and InN. *Journal of Physics: Condensed Matter, 31*(45), 455501.

Wang, W., & Zhao, G. (2012). Lattice vibrations and optical properties of wurtzite InN in the reststrahlen region. *Physica B: Condensed Matter, 407*(21), 4313–4317. https://doi.org/10.1016/j.physb.2012.07.024

Wang, Y., & Li, Z. (2008). First-principles study of the electronic structure and optical properties of cubic boron nitride. *Journal of Physics and Chemistry of Solids, 69*(9), 2367–2370. https://doi.org/10.1016/j.jpcs.2008.05.004

Watanabe, K., Taniguchi, T., & Kanda, H. (2004). Direct-bandgap properties and evidence for ultraviolet lasing of hexagonal boron nitride single crystal. *Nature Materials, 3*(6), 404–409. https://doi.org/10.1038/nmat1134

Wirtz, L., Marini, A., Grüning, M., & Rubio, A. (2006). Excitonic effects in optical absorption and electron-energy loss spectra of hexagonal boron nitride. *Physical Review Letters, 96*(12), 126104. https://doi.org/10.1103/PhysRevLett.96.126104

Wright, A. F. (1997). Elastic properties of zinc-blende and wurtzite AlN, GaN, and InN. *Journal of Applied Physics, 82*(6), 2833–2839. https://doi.org/10.1063/1.366077

Wu, J. (2009). When group-III nitrides go infrared: New properties and perspectives. *Journal of Applied Physics, 106*(1), 011101. https://doi.org/10.1063/1.3155798

Wu, J., Walukiewicz, W., Yu, K. M., Ager, J. W., Haller, E. E., Lu, H., & Schaff, W. J. (2002). Unusual properties of the fundamental band gap of InN. *Applied Physics Letters, 80*(21), 3967–3969. https://doi.org/10.1063/1.1482785

Wu, J., Walukiewicz, W., Yu, K. M., Ager, J. W., Haller, E. E., Lu, H., & Schaff, W. J. (2002). Small band gap bowing in $In_{1-x}Ga_xN$ alloys. *Applied Physics Letters, 80*(25), 4741–4743. https://doi.org/10.1063/1.1485136

Yoshida, S., Hino, T., & Kukimoto, H. (1983). Growth and characterization of GaN crystals. *Journal of Crystal Growth, 59*(1), 217–224. https://doi.org/10.1016/0022-0248(83)90028-4

Zhang, S. B., Wei, S.-H., & Zunger, A. (2001). Intrinsic n-type versus p-type doping asymmetry and the defect physics of GaN. *Journal of Applied Physics, 83*(1), 319–327. https://doi.org/10.1063/1.366771